Available online at www.sciencedirect.com
ScienceDirect
Journal of Catalysis 253 (2008) 105–110
JOURNAL OF CATALYSIS
www.elsevier.com/locate/jcat

Synthesizing mixed-phase TiO_2 nanocomposites using a hydrothermal method for photo-oxidation and photoreduction applications

Gonghu Li [a], Shannon Ciston [b], Zoran V. Saponjic [c], Le Chen [a], Nada M. Dimitrijevic [c], Tijana Rajh [c], Kimberly A. Gray [a,b,*]

[a] *Institute for Catalysis in Energy Processes and Department of Civil and Environmental Engineering, Northwestern University, Evanston, IL 60208, USA*
[b] *Department of Chemical and Biological Engineering, Northwestern University, Evanston, IL 60208, USA*
[c] *Chemical Sciences and Engineering Division and Center for Nanoscale Materials, Argonne National Laboratory, Argonne, IL 60439, USA*

Received 6 July 2007; revised 12 October 2007; accepted 20 October 2007

Available online 26 November 2007

Abstract

Mixed-phase titanium dioxide (TiO_2) materials, such as Degussa P25, show high photocatalytic activity due largely to the synergistic effect between anatase and rutile phases, in which spatial charge separation hinders charge recombination. Our previous studies indicate that a particular nanostructured assembly of anatase and rutile crystallites is necessary for the synergy. In this paper, we apply this structure-function understanding to the synthesis of highly active TiO_2 nanocomposite photocatalysts. Using simple synthetic procedures, we demonstrate an ability to design a highly active nanocomposite that shows enhanced photoactivity in both oxidative and reductive chemistry. Studies by electron paramagnetic resonance spectroscopy indicate the existence of the critical nanostructured assembly and thus the optimization of charge transfer between anatase and rutile phases in the synthesized nanocomposite. These results illustrate the potential of rationally designing photocatalysts for energy applications.

Keywords: Titanium dioxide; Photocatalysis; Mixed-phase; Nanocomposite; CO_2 reduction

1. Introduction

Among the many wide-band semiconductors, titanium dioxide (TiO_2) is an ideal photocatalyst which is stable, inexpensive, safe, and highly reactive [1,2]. Mixed-phase TiO_2 materials consisting of anatase and rutile phases are generally better photocatalysts than pure-phase materials [3–6]. Similar to that of coupled semiconductors, reasoning based on an enhancement of spatial charge separation is usually invoked to explain the high photoactivity of mixed-phase TiO_2. Because the position of the conduction band edge of anatase is higher than that of rutile, photogenerated electrons were assumed to flow from anatase to rutile, while the holes transferred from rutile to anatase [7–9].

Ohno and co-workers observed that oxidation and reduction reactions occurred on rutile and anatase particles, respectively, when mixed-phase TiO_2 was used in photocatalytic oxidation of naphthalene [10]. Electron paramagnetic resonance (EPR) studies by Gray and co-workers indicated that photogenerated electrons actually migrated from rutile to lower energy anatase trapping sites [11–14]. In addition, these authors observed that significantly greater amounts of 2,4,5-trichlorophenol were adsorbed on Degussa P25, a commercial mixed-phase TiO_2 material, than either pure anatase or pure rutile and that charge transfer complexes formed only on Degussa P25 [15,16]. They proposed that the difference between surface reactions on Degussa P25 and those on pure-phase TiO_2 is related to the morphology of Degussa P25, wherein anatase crystallites are interwoven with rutile crystallites and the anatase–rutile interfaces give rise to unique adsorption sites and photocatalytic "hot spots" [16,17].

Mixed-phase TiO_2 materials have been recently fabricated in our lab by chemical and physical methods, including a solvothermal method and reactive DC magnetron sputtering, and have demonstrated excellent photocatalytic activity [18–20]. Whereas most of the studies in the literature report the

* Corresponding author at: Department of Chemical and Biological Engineering, Northwestern University, Evanston, IL 60208, USA.
E-mail address: k-gray@northwestern.edu (K.A. Gray).

0021-9517/$ – see front matter
doi:10.1016/j.jcat.2007.10.014

improved photo-oxidation of organic pollutants by mixed-phase TiO_2 [21–24], it is not clear whether mixed-phase materials also function favorably in reduction reactions. In this work, we investigated the performance of mixed-phase TiO_2 nanocomposites in both oxidative and reductive photochemistry. The nancomposite photocatalysts with a phase composition similar to that of Degussa P25 were prepared by a simple hydrothermal method. The mixed-phase materials were then characterized with various techniques, including EPR, and tested in the oxidation of methylene blue and the reduction of CO_2.

2. Experimental

2.1. Material preparation

The mixed-phase TiO_2 nanocomposites were prepared by a low-temperature hydrothermal method [18]. The protocol involved synthesis of rutile nanocrystals in the presence of commercially available anatase powder (Sigma–Aldrich, 99.8%). Before the hydrothermal process, 2.0 ml of titanium (IV) chloride (Sigma–Aldrich, 99.9%) was hydrolyzed in an 80-ml solution of 2 M hydrochloric acid. After stirring at room temperature for 90 min, a clear solution was obtained, which was mixed thoroughly with 4.0 g of anatase powder and 1.0 ml of 5 v/v% Triton X-100 (Baker) in ethanol. Then the mixture was transferred to a 250-ml flask and refluxed at 373 K for 22 h. The resulting nanocomposite in the flask was centrifuged, washed with water, and dried at room temperature. The mixed-phase TiO_2 in powder form thus obtained was sintered in air at 773 K for 4 h to remove residual organics, improve crystallinity, and develop better anatase–rutile interface.

In what follows, the synthesized mixed-phase materials before and after sintering at 773 K are designated anatase–rutile 373 K and anatase–rutile 773 K, respectively. Using the same synthetic conditions, rutile nanocrystals also were synthesized in the absence of the commercial anatase. The synthesized rutile and commercial anatase were sintered at 773 K for 4 h, and were designated rutile 773 K and anatase 773 K, respectively. The commercial anatase and mixed-phase nanocomposite also were sintered at 1073 K to probe the effect of high-temperature treatment on the phase structures and photocatalytic properties of the TiO_2 materials. Degussa P25 was used as received. Milli-Q water with a resistivity of 18 MΩ/cm was used in the catalyst preparation and photocatalytic testing.

2.2. Material characterization

The synthesized mixed-phase nanocomposites and other photocatalysts were characterized by X-ray diffraction (XRD), scanning electron microscopy (SEM), and EPR spectroscopy. The XRD patterns of powder samples were recorded on a Rigaku XDS 2000 diffractometer using nickel-filtered Cu$K\alpha$ radiation ($\lambda = 1.5418$ Å) over a range of $20° < 2\theta < 60°$. A Hitachi S-4500 scanning electron microscope equipped with a cold field emission electron gun was used for imaging the synthesized photocatalysts. EPR spectra were collected on a Bruker ELEXSYS E580 spectrometer equipped with a helium cryostat. For EPR studies, samples dispersed in Milli-Q water were purged with nitrogen, cooled to 5 K, and illuminated within the cavity at that temperature while spectra were acquired. A 300-W xenon lamp (ILC Inc.) was used as the light source for EPR studies. The g tensor values were calibrated for homogeneity and accuracy by comparison with a coal standard ($g = 2.00285 \pm 0.00005$). Specific surface areas of the photocatalysts were obtained on a Quantachrome Nova 1200 multipoint BET apparatus using approximately 200 mg of sample for each measurement.

2.3. Photocatalytic testing

The photodegradation of methylene blue was carried out in a batch mode reactor, in which 10 mg of photocatalyst was mixed with a 100-ml solution of 5 mg/L methylene blue (Merck, USP). The slurry was then irradiated with a 100-W mercury spot lamp (UVP). Every 4 min, the reaction solution was sampled and separated from the photocatalyst using a GHP Acrodisc 13-mm syringe filter with a 0.45-μm GHP membrane (Pall). The absorbance of methylene blue at 660 nm was monitored using a Hitachi U-2000 UV–visible spectrophotometer. According to Beer's law, the concentration of methylene blue is proportional to absorbance at 660 nm.

A commercial annular reactor (ACE Glass, Vineland, NJ), comprising a glass reaction vessel and a quartz immersion well as the cooling jacket, was used for the photoreduction of CO_2 [13]. A 450-W medium-pressure mercury arc lamp (Hanovia), providing UV/visible light irradiation, was encased in the quartz immersion well in the center of the reaction vessel. In a typical run, 500 mg of photocatalyst was dispersed in Milli-Q water by sonication before being transferred to the reaction vessel. Together with 100 mg of sodium bicarbonate (Mallinckrodt, AR) and 1.0 ml of isopropanol (Acros Organics, 99.5%), Milli-Q water was added to the reaction vessel, making volumes of the solution and the head space above the solution of 1000 and 280 ml, respectively. Before photochemical reactions, gaseous CO_2 (Airgas, industrial grade) was bubbled through the reaction vessel for 1 h. Then the reactor was tightly sealed before the photochemical reaction was started. During the reaction process, cooling water was run through the quartz immersion well. The reaction solution was stirred continuously while the temperature of the solution was maintained between 293 and 298 K. The gas phase above the reaction solution was sampled periodically for analysis using an HP 5890 gas chromatograph equipped with a flame ionization detector. A GOW-MAC 580 gas chromatograph equipped with a thermal conductivity detector and a Hitachi high-performance liquid chromatograph were adopted to detect carbon monoxide in the gas phase and organic products in the solution, respectively.

3. Results and discussion

3.1. Characterization of the synthesized TiO_2 nanocomposites

The hydrothermal method is a low-cost and convenient, yet robust method for the synthesis and morphological transformation of many nanostructures [25]. It has been shown that the

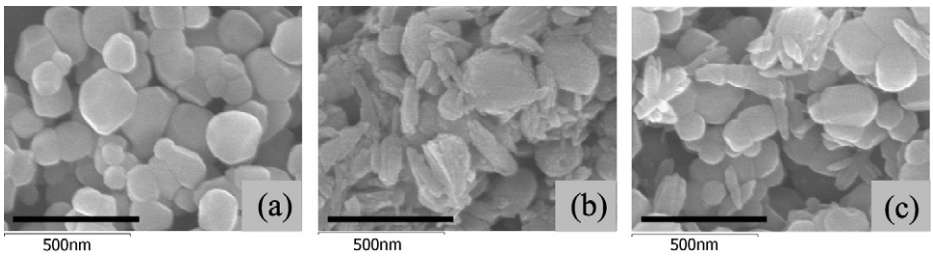

Fig. 1. Electron micrographs of (a) the commercial anatase, (b) anatase–rutile 373 K, and (c) anatase–rutile 773 K (scale bar 500 nm).

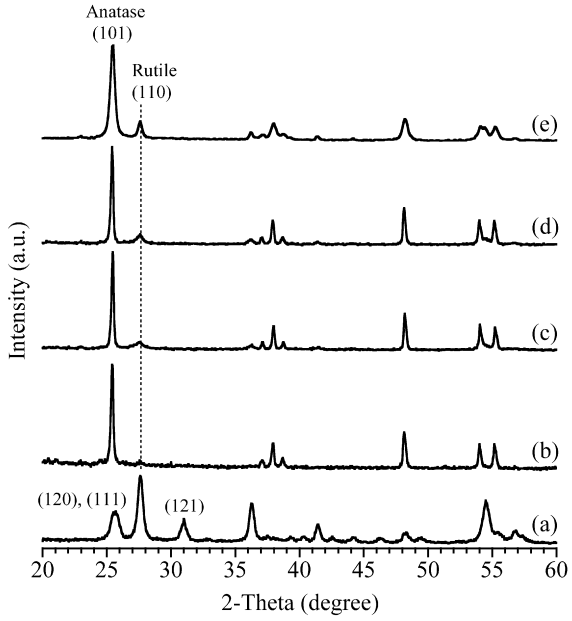

Fig. 2. XRD patterns of (a) rutile 773 K, (b) anatase 773 K, (c) anatase–rutile 373 K, (d) anatase–rutile 773 K, and (e) Degussa P25. The diffraction peaks of anatase (101), rutile (110), and brookite (120), (111), (121) faces are labeled.

phase composition of TiO_2 materials can be tuned by varying synthetic parameters, such as acidity and water content, in the hydrothermal process [18,26]. In our study, mixed-phase photocatalysts were obtained by synthesizing rutile nanocrystals by the hydrothermal method in the presence of commercial anatase powders. Fig. 1 shows SEM images of the commercial anatase (Fig. 1a), synthesized anatase–rutile 373 K (Fig. 1b), and anatase–rutile 773 K (Fig. 1c). As can be seen, rutile nanocrystals synthesized in the presence of commercial anatase powder were rod-like and, on sintering at 773 K, became attached to the spherical anatase particles.

The crystal structure of the synthesized nanocomposites was determined by XRD. Fig. 2 shows the XRD patterns of different TiO_2 materials. In the absence of the commercial anatase, rutile nanocrystals with a significant amount of brookite were synthesized by the hydrothermal method, as indicated by the diffraction patterns of rutile (110) and brookite (120), (111), (121) faces (Fig. 2a). The XRD diffraction patterns shown in Figs. 2b–2d indicate that rutile nanocrystals were successfully synthesized by the hydrothermal method in the presence of the commercial anatase. As mentioned earlier, the nanocomposite was sintered at 773 K to improve crystallinity. This improved crystallinity was confirmed by the fact that the rutile (110) diffraction peak was narrower for anatase–rutile 773 K (Fig. 2d) compared with anatase–rutile 373 K (Fig. 2c). The diffraction patterns also indicate that the synthesized nanocomposites had a similar phase composition as Degussa P25 (∼80% anatase and ∼20% rutile), and that the presence of brookite phase was negligible. The bulk crystal phase of the commercial anatase did not change after sintering at 773 K for 4 h (Fig. 2b), nor did its photoactivity change with sintering to any substantial extent. In addition, the phase proportions, as evaluated by XRD, of both the commercial anatase and the synthesized nanocomposite did not change significantly after sintering at even higher temperatures, such as 1073 K.

3.2. *Photocatalytic activity of the mixed-phase TiO_2 nanocomposites*

The photo-oxidation of methylene blue under UV illumination was used to evaluate the photoactivity of the synthesized mixed-phase photocatalysts. The characteristic absorbance at 660 nm of the methylene blue solution was monitored during the reaction process. As can be seen from Fig. 3, rutile 773 K appeared to be a poor photocatalyst. The simple addition of rutile nanocrystals by the hydrothermal method did not improve the photoactivity of the commercial anatase, because the methylene blue decay in the presence of anatase–rutile 373 K was slower than that in the presence of anatase 773 K. However, the nanocomposite after sintering at 773 K (anatase–rutile 773 K) demonstrated the highest photoactivity among the catalysts tested in this study. Thermal treatment at a higher temperature (1073 K) did not further improve the photocatalytic activity of the synthesized nanocomposite. Fig. 3 shows that the shapes of the decay curves for anatase 773 K and anatase–rutile 773 K were different from those of Degussa P25 and anatase–rutile 373 K. This may indicate that the initial reaction rates of methylene blue decay were much higher in the presence of the former two photocatalysts than in the presence of latter two.

Anatase–rutile 773 K also was tested as a photocatalyst for CO_2 reduction under UV/visible light illumination. The photoreduction of CO_2 to CO or energy-rich fuels such as CH_4 and CH_3OH is considered a sustainable mode of synthesis, because solar energy could be used as the renewable energy input for the chemical conversion [27]. In our study, methane was detected as the major gas-phase product (>90% selectivity) with ethane as the minor product. Other compounds that could form during CO_2 reduction, such as carbon monoxide and formic acid [28–30], were not detectable under the experimental conditions described in this paper. Fig. 4 compares the formation of

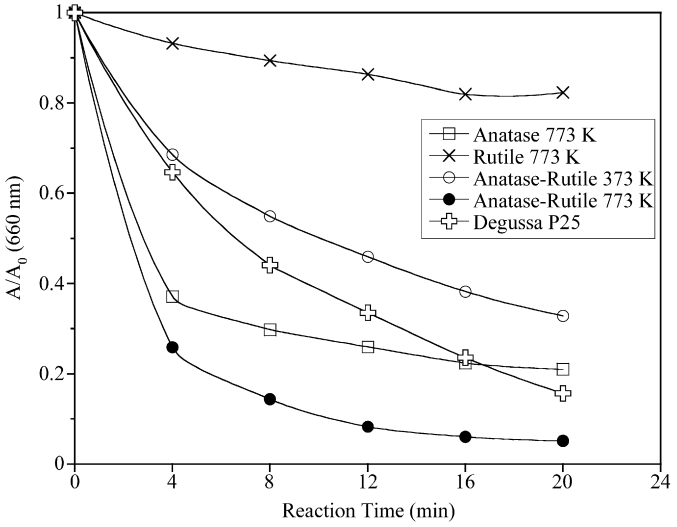

Fig. 3. Normalized absorbance of methylene blue at 660 nm as a function of reaction time during photocatalytic oxidation under UV illumination.

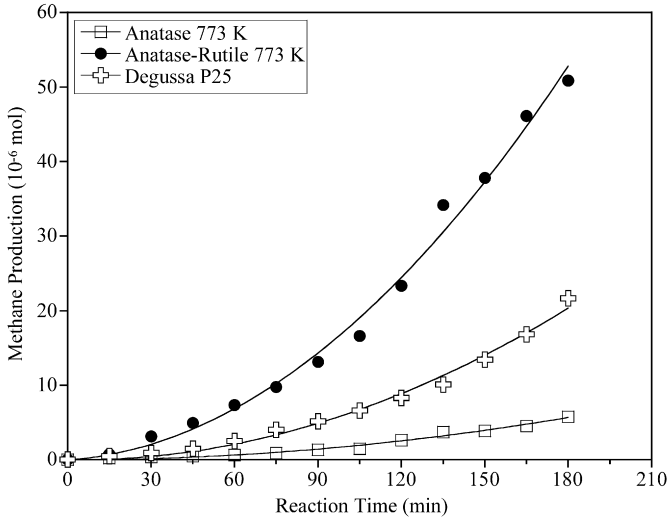

Fig. 4. Methane production during the photoreduction of carbon dioxide in the presence of isopropanol as a hole scavenger. The reaction was carried out under UV/visible light illumination. The temperature of reaction solutions was controlled to be between 293 and 298 K.

methane as a function of reaction time during CO_2 reduction using different photocatalysts. As can be seen, the photoactivity of the commercial anatase toward CO_2 reduction was significantly improved by forming a nanocomposite with rutile. In addition, anatase–rutile 773 K also led to much greater rate of methane formation than Degussa P25, the gold standard for photocatalysts.

3.3. EPR studies of the mixed-phase TiO_2 photocatalysts

As demonstrated by comparing Figs. 3 and 4, anatase–rutile 773 K was more active than anatase–rutile 373 K in both methylene blue degradation and CO_2 reduction, suggesting that thermal treatment at 773 K is very important for the high photoactivity of the anatase–rutile nanocomposite. Sintering at high temperatures usually leads to decreased surface areas and improved crystallinity (decreased recombination) of TiO_2 photocatalysts [31,32]. In this study, the specific surface areas of the commercial anatase and anatase–rutile 773 K were 8.6 and 11.5 m^2/g, respectively. However, surface area does not account for the difference in photoactivity, because Degussa P25 has a greater surface area ($\sim$50 m^2/g) [33] but lower photoactivity than anatase–rutile 773 K. The improved crystallinity of rutile nanocrystals after sintering at 773 K may contribute to the superior activity of anatase–rutile 773 K by reducing charge recombination, which tends to occur to a greater degree in TiO_2 materials with lower crystallinity.

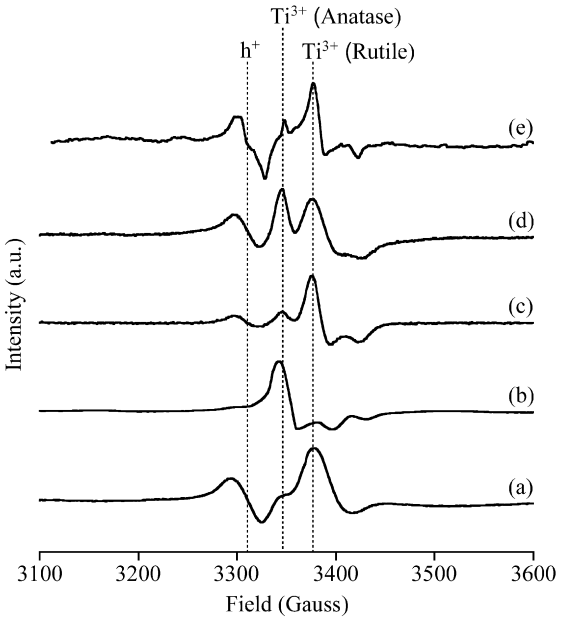

Fig. 5. Difference EPR spectra of (a) rutile 773 K, (b) the commercial anatase, (c) anatase–rutile 373 K, (d) anatase–rutile 773 K, and (e) Degussa P25. Background spectra in dark have been subtracted from the corresponding spectra under UV/visible light illumination. Electrons trapped (Ti^{3+}) in both anatase and rutile and trapped holes (h^+) are labeled.

The anatase–rutile nanocomposites were further studied with low-temperature EPR spectroscopy, providing unambiguous identification of the species involved in the charge separation processes and enabling the identification of charge-trapping sites in TiO_2 materials. The EPR spectra of various TiO_2 materials under UV/visible light illumination are shown in Fig. 5. Two prominent signals corresponding to trapped holes (h^+, $g = 2.014$) and trapped electrons in rutile lattice (Ti^{3+}, $g_\perp = 1.975$) can be seen for rutile 773 K, as shown in Fig. 5a. A resonance characteristic of electrons trapped in anatase lattice (Ti^{3+}, $g_\perp = 1.990$) was present in the EPR spectrum of the commercial anatase (Fig. 5b) [12]. Both electron signals in anatase and in rutile can be seen in the EPR spectra of mixed-phase materials with similar phase composition (Figs. 5c–5e). The EPR spectrum of anatase–rutile 373 K (Fig. 5c) under continuous UV/visible light irradiation was similar to that of Degussa P25 (Fig. 5e), which is consistent with those reported in the literature [12]. Anatase–rutile 773 K, although having a similar phase composition as anatase–rutile 373 K and Degussa P25, shows a different charge-trapping pattern (Fig. 5d).

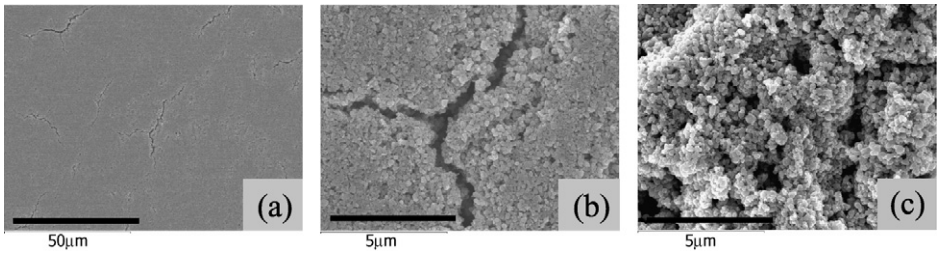

Fig. 6. Electron micrographs of (a) a film prepared from anatase–rutile 373 K (scale bar 50 μm), (b) the same film as in (a) at a higher magnification (scale bar 5 μm), and (c) a film prepared from anatase–rutile 373 K after sintering at 773 K (scale bar 5 μm).

As discussed earlier, photogenerated electrons in Degussa P25 migrated from rutile to lower-energy anatase-trapping sites in a particular small fraction [12,13]. In the small-size fraction, anatase crystallites were interwoven with rutile crystallites to create a nanostructured aggregate that promoted electron transfer from rutile to anatase-trapping sites and stabilized charge separation. This spatial charge separation was correlated with the photocatalytic activity of size-fractioned Degussa P25 in phenol degradation [13]. In this present study, the EPR signature of anatase–rutile 773 K (Fig. 5d) was very similar to that of the more active and smaller-size fraction of Degussa P25 [12]. Anatase–rutile 773 K demonstrated superior photoactivity in both oxidation and reduction reactions. Thus, our study illustrates a targeted synthesis of a nanostructured assembly bearing the critical characteristics that we hypothesize to explain the high activity of Degussa P25. We suggest that the excellent photoactivity of anatase–rutile 773 K was due to the effective charge separation occurring between phases in this nanostructured assembly. The lack of such charge separation in anatase–rutile 373 K likely was due to the absence of strong attachment or connection between anatase and rutile before sintering at 773 K.

3.4. Synthesis-structure-function relationships for TiO_2 photocatalysts

The photocatalytic activity of TiO_2 materials can be influenced by many factors, including crystal structure, particle size, surface area, porosity, density of surface hydroxyl groups, surface acidity, number and nature of trap sites, and adsorption–desorption characteristics [25]. Although we have demonstrated that spatial charge separation contributed to the improved photoactivity of anatase–rutile 773 K, other factors exist that should not be ignored. The hydrothermal treatment potentially improves the activity of some TiO_2 photocatalysts. For example, it has been suggested that the photoactivity of Degussa P25 was enhanced due to the formation of additional surface hydroxyl groups after hydrothermal treatment at 423 K [34]. Solvent treatment of Degussa P25 also was found to affect the efficiency of solar energy conversion when the TiO_2 material was used in dye-sensitized solar cells [35]. In our study, however, no appreciable improvement in photoactivity was observed for the commercial anatase after hydrothermal treatment at 373 K. Rather, the rutile nanocrystals synthesized by the hydrothermal method were found to function as an activating "glue" binding anatase particles together. Such hydrothermal processing could potentially be used to fabricate reactive membranes. As can be seen in Fig. 6a, a smooth film was obtained by simply dispersing and drying anatase–rutile 373 K on a glass slide. Close examination of the film indicates that commercial anatase particles were incorporated into the film and were well mixed with rutile nanocrystals (Fig. 6b; also see Fig. 1b). Using a similar protocol, Chen and co-workers prepared photocatalytic films containing Degussa P25 on stainless steel through a sol–gel method [36,37]. In addition, the SEM image shown in Fig. 6c reveals that a three-dimensional mesoporous structure formed on sintering the film of anatase–rutile 373 K. Such porous structures were not observed for anatase–rutile nanocomposites that were synthesized without using surfactant and demonstrated slightly lower photoactivity than anatase–rutile 773 K. Thus, the porosity originated from the use of surfactant during the hydrothermal synthesis and also contributed to the enhanced photoactivity of anatase–rutile 773 K.

The connection and interfacial morphology between TiO_2 nanocrystals have been identified as important parameters that could significantly alter the properties of TiO_2-based nanocomposites in various applications [14]. In a recent study by Elser and co-workers, isolated anatase nanocrystals were brought together by hydrating and subsequently dehydrating the nanocrystals at 473 K [38]. They detected the presence of polarizable conduction band electrons in the nanocrystal assemble and revealed that the energy needed for defect formation at grain boundaries was substantially reduced after the hydration–dehydration treatment [38]. We have shown that a simple hydrothermal process followed by thermal treatment renders a nanocomposite photocatalyst with high activity. The interfacial morphology in the nanocomposite was optimized by thermal treatment at 773 K, which also may create defect sites at the phase interface between anatase and rutile. This approach may be adapted in developing TiO_2 nanostructures for energy applications, such as dye-sensitized solar cells, that require rapid and efficient electron migration across the phase interface (or grain boundaries) between TiO_2 nanocrystals.

4. Conclusions

Despite the wide interest and intensive research in the field of TiO_2 photocatalysis, there are only a few studies in the literature regarding the synthesis-structure-function relationships for TiO_2-based materials. Previous results suggest that the enhanced activity of Degussa P25 is due to the fraction of bulk material having a nanostructured arrangement of inter-

woven anatase–rutile crystallites where (i) rutile extends photoresponse to the visible light region, (ii) charge recombination is hindered by charge transfer and separation across phase interface, and (iii) unique interfacial trapping sites exist and are possibly photocatalytic "hot spots." The present study demonstrates the successful attempt at a targeted synthesis of such an anatase–rutile nanocomposite, which is serendipitously formed in Degussa P25 but enhances both oxidative and reductive photochemistry.

In this study, a mixed-phase photocatalyst was prepared by forming a nanocomposite between anatase and rutile via a simple hydrothermal method followed by sintering at 773 K. The mixed-phase nanocomposite showed higher activity than Degussa P25 in both oxidation and reduction reactions. The nanocomposite demonstrated electron trapping/transfer behavior characteristic of the particular nanostructured assembly that is responsible for the high photoactivity of Degussa P25. The effective charge separation between anatase and rutile phases was shown to contribute to the superior photoactivity of the synthesized mixed-phase TiO_2 nanocomposite. The results described in this paper provide insights into the role of solid–solid interface in TiO_2 photocatalysis and also a feasible mode of preparing highly active photocatalytic materials.

Acknowledgments

The authors thank the U.S. Department of Energy (contracts DE-FG02-03ER15457/A003 and DE-AC02-06CH11357) and National Science Foundation (grant BES-0403581) for funding the research described in this paper. The EPR work at Argonne National Laboratory was performed under the auspices of the U.S. Department of Energy, Office of Basic Energy Sciences, Division of Chemical Sciences, Geosciences and Biosciences, under contract DE-AC02-06CH11357. The authors also thank Dr. Kevin Knagge and Professor Vicki H. Grassian of the University of Iowa for their help with BET surface area measurements. Characterization by XRD and SEM was performed in the MRSEC and NUANCE center at Northwestern University.

References

[1] T. Thompson, J. Yates Jr., Chem. Rev. 106 (2006) 4428.
[2] U. Diebold, Surf. Sci. Reports 48 (2003) 53.
[3] T. Ohno, K. Sarukawa, K. Tokieda, M. Matsumura, J. Catal. 203 (2001) 82.
[4] T. Kawahara, Y. Konishi, H. Tada, N. Tohge, J. Nishii, S. Ito, Angew. Chem. Int. Ed. 41 (2002) 2811.
[5] Q. Shen, K. Katayama, T. Sawada, M. Yamaguchi, Y. Kumagai, T. Toyoda, Chem. Phys. Lett. 419 (2006) 464.
[6] B. Sun, P. Smirniotis, Catal. Today 88 (2003) 49.
[7] H. Nakajima, T. Mori, Q. Shen, T. Toyoda, Chem. Phys. Lett. 409 (2005) 81.
[8] M. Yan, F. Chen, J. Zhang, M. Anpo, J. Phys. Chem. B 109 (2005) 8673.
[9] R. Bickley, T. Gonzalezcarreno, J. Lees, L. Palmisano, R. Tilley, J. Solid State Chem. 92 (1991) 178.
[10] T. Ohno, K. Tokieda, S. Higashida, M. Matsumura, Appl. Catal. A 244 (2003) 383.
[11] D. Hurum, K. Gray, T. Rajh, M. Thurnauer, J. Phys. Chem. B 109 (2005) 977.
[12] D. Hurum, A. Agrios, K. Gray, T. Rajh, M. Thurnauer, J. Phys. Chem. B 107 (2003) 4545.
[13] D. Hurum, A. Agrios, S. Crist, K. Gray, T. Rajh, M. Thurnauer, J. Electron Spectrosc. Relat. Phenom. 150 (2006) 155.
[14] G. Li, K. Gray, Chem. Phys. 339 (2007) 173.
[15] D. Hurum, K. Gray, T. Rajh, M. Thurnauer, J. Phys. Chem. B 108 (2004) 16483.
[16] A. Agrios, K. Gray, E. Weitz, Langmuir 19 (2003) 1402.
[17] A. Agrios, K. Gray, E. Weitz, Langmuir 20 (2004) 5911.
[18] G. Li, K. Gray, Chem. Mater. 19 (2007) 1143.
[19] L. Chen, M. Graham, G. Li, K. Gray, Thin Solid Films 515 (2006) 1176.
[20] G. Li, L. Chen, M. Graham, K. Gray, J. Mol. Catal. A 275 (2007) 30.
[21] Y. Kolen'ko, B. Churagulov, M. Kunst, L. Mazerolles, C. Colbeau-Justin, Appl. Catal. B 54 (2004) 51.
[22] S. Bakardjieva, J. Subrt, V. Stengl, M. Dianez, M. Sayagues, Appl. Catal. B 58 (2005) 193.
[23] T. Kawahara, T. Ozawa, M. Iwasaki, H. Tada, S. Ito, J. Colloid Interface Sci. 267 (2003) 377.
[24] R. Bacsa, J. Kiwi, Appl. Catal. B 16 (1998) 19.
[25] O. Carp, C. Huisman, A. Reller, Prog. Solid State Chem. 32 (2004) 33.
[26] C. Wang, J. Ying, Chem. Mater. 11 (1999) 3113.
[27] C. Song, Catal. Today 115 (2006) 2.
[28] T. Inoue, A. Fujishima, S. Konishi, K. Honda, Nature 277 (1979) 637.
[29] P. Usubharatana, D. McMartin, A. Veawab, P. Tontiwachwuthikul, Ind. Eng. Chem. Res. 45 (2006) 2558.
[30] H. Yoneyama, Catal. Today 39 (1997) 169.
[31] A. Agrios, P. Pichat, J. Photochem. Photobiol. A 180 (2006) 130.
[32] R. Enriquez, A. Agrios, P. Pichat, Catal. Today 120 (2007) 196.
[33] A. Mills, S. LeHunte, J. Photochem. Photobiol. A 108 (1997) 1.
[34] J. Yu, H. Yu, B. Cheng, M. Zhou, X. Zhao, J. Mol. Catal. A 253 (2006) 112.
[35] D. Zhang, J. Downing, F. Knorr, J. McHale, J. Phys. Chem. B 110 (2006) 21890.
[36] Y. Chen, D. Dionysiou, Appl. Catal. A 317 (2007) 129.
[37] Y. Chen, D. Dionysiou, Appl. Catal. B 62 (2006) 255.
[38] M. Elser, T. Berger, D. Brandhuber, J. Bernardi, O. Diwald, E. Knoezinger, J. Phys. Chem. B 110 (2006) 7605.